RSC Advances

PAPER

View Article Online
View Journal | View Issue

Cite this: *RSC Adv.*, 2023, **13**, 34598

A heterostructural MoS_2QDs@UiO-66 nanocomposite for the highly efficient photocatalytic degradation of methylene blue under visible light and simulated sunlight†

A. M. Aboraia, *[aij] Majd Al-omoush,[b] Malak Solayman,[b] Hatem M. H. Saad,[c] Gomaa Khabiri,[d] Mohamed Saad,[e] Ghayah M. Alsulaim,[f] Alexander V. Soldatov,[b] Yasser A. M. Ismail*[g] and H. Gomaa[h]

The development of recyclable photocatalysts with high activity and stability has piqued the interest of researchers in the field of wastewater treatment. In this study, an ultrasonic probe approach was used to immerse a sequence of heterojunctions formed by metal–organic frameworks (UiO-66) and different amounts of molybdenum disulfide quantum dots (MoS_2QDs), resulting in a highly recyclable MoS_2QDs@UiO-66 photocatalyst. Multiple advanced techniques, such as XPS, XRD, TEM, XRF, and UV-vis spectrophotometry, were used to characterize and confirm the successful preparation of UIO-66 impregnated with MoS_2QDs. The results indicated that the best heterostructure catalyst exhibited superior efficiency in the photocatalytic degradation of methylene blue (MB) in water, achieving approximately 99% removal within 30 minutes under simulated sunlight, while approximately 97% removal under visible light. The outstanding photocatalytic performance is predominantly attributed to the photoinduced separation of carriers in this heterostructure system. This study proposes a unique, simple, and low-cost method for improving the degradation performance of organic contaminants in water.

Received 15th September 2023
Accepted 2nd November 2023

DOI: 10.1039/d3ra06299f

rsc.li/rsc-advances

1. Introduction

Photocatalysis of the semiconductor material is a powerful process for environmental detoxification that converts hazardous and non-biodegradable organic molecules to carbon dioxide, inorganic salts, and water.[1–5] Metal–organic frameworks (MOFs), which are porous structures consisting of metal building units and organic bridging ligands, have been identified as possible photocatalysts.[6,7] Metal–organic frameworks (MOFs) with high porosity display semiconducting properties when exposed to sunlight, suggesting they might be used as photocatalysts.[5,8,9] As a result of their semiconducting nature, they might be viable options for wastewater treatment. Additionally, their catalytic capabilities can be used for the environment-friendly reduction of hazardous chemical compounds. Most MOFs cannot absorb visible light or do not have enough catalytic sites to photocatalytically produce H_2.[10,11] Two typical methods have been used for the production of photocatalytically active MOFs. The first method is doping MOFs with light-absorbing metal complexes. The second method involves including light-absorbing organic building blocks into MOFs, for instance, porphyrins and 2-amino terephthalate, to capture visible light. Water pollution degradation, water splitting, CO_2 reduction, and organic synthesis are examples of photocatalytic MOF solar-driven applications.[12,13]

UiOs are classified as a stable group of MOFs. The zirconium-based MOF UiO-66 exhibits high porosity[14,15] as well as has high thermal, water, and acid stability (acetone, benzene, and DMF). UiO-66 is extremely versatile in its functionalization and

[a]Department of Physics, Faculty of Science, Al-Azhar University, Assiut, 71542, Egypt. E-mail: a.m.aboraia@gmail.com
[b]Smart Materials Research Institute, Southern Federal University, Sladkova 178/24, 344090, Rostov-on-Don, Russia
[c]Capability Systems Centre School of Engineering and IT, The University of New South Wales Canberra, ACT, Australia
[d]Physics Department, Faculty of Science, Fayoum University, Fayoum, 63514, Egypt
[e]Department of Radiological Science, Faculty of Applied Medical Science, King Khalid University, P. O. Box 9004, Abha, Saudi Arabia
[f]Department of Chemistry, Faculty of Science, King Faisal University, Al Ahsa, Saudi Arabia
[g]Department of Physics, Faculty of Science, Islamic University of Madinah, Saudi Arabia. E-mail: Yasser_ami@yahoo.com
[h]Department of Chemistry, Faculty of Science, Al-Azhar University, Assiut, 71542, Egypt
[i]Energy Storage Research Laboratory (ESRL), Physics Department, Faculty of Science, Al-Azhar University, Assiut 71542, Egypt
[j]College of Industry and Energy Technology, New Assiut Technological University, New Assiut City, Assiut, Egypt

† Electronic supplementary information (ESI) available. See DOI: https://doi.org/10.1039/d3ra06299f

application. However, the adsorption of dyes from solution on MOFs has rarely been studied.[16,17] Moreover, UiO-66, compared to other inorganic catalysts, fails to reach reasonable photocatalytic performances owing to light absorption. Thus, to enhance the efficiency of the UiO-66 family photocatalyst, several composites, such as CdSe quantum dots, have been added to UiO-66 to remove the RHB dye. In addition, nanoparticles of Au were added to the pure sample. The above results signify that the UiO-66 analogies are worthy candidates as photocatalysts. Also, other QDs@MOF composite photocatalysts have been reported, such as CdS/MIL-101,[18] CdS/MIL-125, and MoS_2QDs@UiO-66–NH_2/G, where MoS_2QDs effectively increased the photo-generated charge carriers and electron transport, resulting in a significant increase in photocatalytic hydrogen evolution.[19] Therefore, it can be supposed that MoS_2QDs and UiO-66 can complement each other to overcome the limitations of individual materials. Since Mo is a mandatory element for both plants and animals, this technique is environment-friendly and is appropriate for large-scale preparation.[20]

Here, we first describe the use of UiO-66@MoS_2QDs as a photocatalyst with visible-light activity and its application in water treatment. The primary goal of this research is to create a UiO-66@MoS_2QDs compound with desirable photocatalytic capabilities and adequate stability for organic dye degradation. The UiO-66@MoS_2QDs photocatalyst was created using a straightforward solution approach in which UiO-66 served as both, a substrate and a mediator, for the synthesis of MoS_2QDs. The photocatalytic activity of UiO-66@MoS_2QDs photocatalyst was tested by degrading MB under both simulated and real sunlight irradiation. In addition, the photocatalytic mechanism and photocatalyst recycling are discussed.

2. Experimental method

2.1. Chemicals

1,4-benzenedicarboxylic acid, 1,4-naphthalenedicarboxylic acid, zirconium tetrachloride, terephthalic acid (H_2BDC), *N*,*N*-dimethylformamide (DMF), benzoic acid (BA), ammonium molybdate, thiourea, isopropanol, and MB were acquired from Alfa Aesar and utilized without additional purification.

2.2. Characterizations tools

The elemental structure and binding behavior of the UiO-66@MoS_2QDs photocatalyst were analyzed using X-ray photoelectron spectroscopy (XPS; Thermo-Fisher Sci., USA). The structural properties of UiO-66@MoS_2QDs samples were studied using X-ray diffraction (XRD), a D2 Phaser instrument, employing CuK_α radiation (wavelength is equal to 1.540598 Å). The microstructure of these samples was investigated using TEM on the FEI Tecnai G2 Spirit TWIN instrument operating at 80 kV. The elemental chemical analysis of UiO-66@MoS_2QDs samples was examined employing a Bruker M4-Tornado X-ray fluorescence (XRF) instrument. The energy gap was computed by measuring the absorbance using a Shimadzu UV-2600 instrument with λ ranging from 190 to 900 nm.

2.3. Synthesis of UiO-66@MoS_2QDs photocatalyst

UiO-66 was synthesized following our previous report.[21] $ZrCl_4$ was dispersed in DMF and some drops of deionized water were added to the reaction. Then, benzoic acid was added until a clear solution was achieved. The clear solution was placed in a preheated oven for crystallization at ~120 °C for one day. The as-prepared MoS_2 was synthesized based on our previous work.[22] To fabricate UiO-66 impregnated by MoS_2QDs, a simple approach of ultrasonic mixing route was used; firstly, 50 mg of UiO-66 was well dispersed in 30 mL of deionized water. Different concentrations of MoS_2QDs were added, and the mixture was then exposed to ultrasonic waves for a further one hour. The product was washed several times and then dried overnight at 60 °C to obtain UiO-66@MoS_2QDs.

2.4. The photocatalytic performance of UiO-66@MoS_2QDs

Under UV irradiation, photocatalytic studies of UiO-66@MoS_2-QDs were evaluated for MB degradation. In the typical experimental methodology, 25 mg of UiO-66@MoS_2QDs was contacted with 50 mL of MB-dye (10 ppm) solution. When the filtration was completed, the material was centrifuged at 5000 rpm for 10 min before examining it using UV-vis spectroscopy. The UiO-66@MoS_2QDs photocatalyst and the solution of MB were mixed for 30 min in the dark box before exposure to radiation to complete the adsorption process and desorption equilibrium. UiO-66@MoS_2QDs adsorbed with MB molecules resulted in a forthright reaction of MB with electron plus hole pairs. A closed dark reactor was employed, with a 10 cm gap between the UV lamp and the MB–UiO-66@MoS_2QDs beaker. To measure the catalytic effect under real sung light for MB,[23,24] 50 mg of the photocatalyst was added to 0.010 L of the MB dye solution (10 mg L^{-1}) in the reactor independently. Before irradiation, we followed the same protocol for the simulated sunlight since the mixture was mixed for 180 seconds in the dark to realize an adsorption/desorption equilibrium for the dye as well as photocatalysts. After half an hour in the dark, the solution was exposed to sunlight under continuous stirring. The photocatalysis experiment involving the MB dye was performed outside in the solar light on a sunny day in October from 12 a.m. and 3 p.m. where the solar intensity was 7.2–7.8 kW h per m^2 per day at the Al-Azhar University, Assiut, Egypt. At a specified time interval, ~3 mL of the solution was separated from the reactor and centrifuged to separate the catalysts by analysis. The absorbance of the MB solution at 665 nm was also measured to test MB photodegradation. To compute the efficiency of photodegradation/removal, the following equation was used:[25]

$$\text{Removal}\% = \frac{(C_i - C_f)}{C_i} \times 100$$

Following the completion of the photocatalytic degradation process, the starting and final MB concentrations (C_i and C_f) were calculated. A series of photocatalytic experiments were conducted to determine the effects of pH, contact length, dose, and temperature on photocatalytic activity. After the photocatalytic procedure was completed, the consumed UiO-

66@MoS_2QDs was collected and mixed with 0.1 M HNO_3 before rinsing twice with DI water under ultrasonic conditions to eliminate any residual MB. The regenerated photocatalyst UiO-66@MoS_2QDs can be used up to six times with outstanding efficiency.

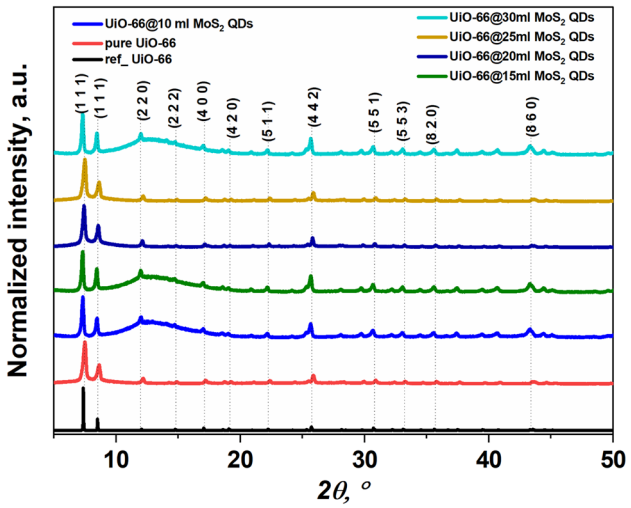

Fig. 1 The XRD powder patterns of the samples ref UiO-66 (the information card for entry #4512072 (crystallography open database)), pure UiO-66, and UiO-66@MoS_2QDs at different amounts of MoS_2-QDs (10, 15, 20, 25, and 30 mL).

3. Result and discussion

3.1. Characterization of the UiO-66@MoS_2QDs photocatalyst

The refined powder XRDs of pristine UiO-66 and UiO-66 coated with different concentrations of MoS_2 quantum dots are shown in Fig. 1. X-ray diffraction proved that all samples have a single cubic phase ($Fm\bar{3}m$) according to the information card for entry #4512072 (crystallography open database). All peaks were indexed for UiO-66 without any impurities from other peaks linked to other phases. Moreover, for UiO-66@MoS_2QDs, no additional peaks correspond to MoS_2 due to the small amount of MoS_2. As shown in Fig. 2a–f, the size and microstructure of the pure UiO-66 NPs, as well as the UiO-66 coating with varied MoS_2QD levels, were determined by TEM. According to Fig. 2a, the average size of the smooth cubic crystal of pure UiO-66 was less than 100 nm, and the average size for all samples was less than 100 nm. Although the nanoparticles of UiO-66 are small, they seem to be agglomerated and have a large particle size. Additionally, TEM images of UiO-66@MoS_2QD nanocomposites displayed that the QDS of the MoS_2 was efficiently and successfully connected to the UiO-66 surface, which benefitted the charge carrier transfer in the heterostructures, as a result, it could enhance the photocatalytic activity of the UiO-66@MoS_2QDs nanocomposites, as illustrated in Fig. 3b–f. For further confirmation of MoS_2, the samples were analyzed by XRF, and the concentrations of each element were exhibited, as shown in Table 1.

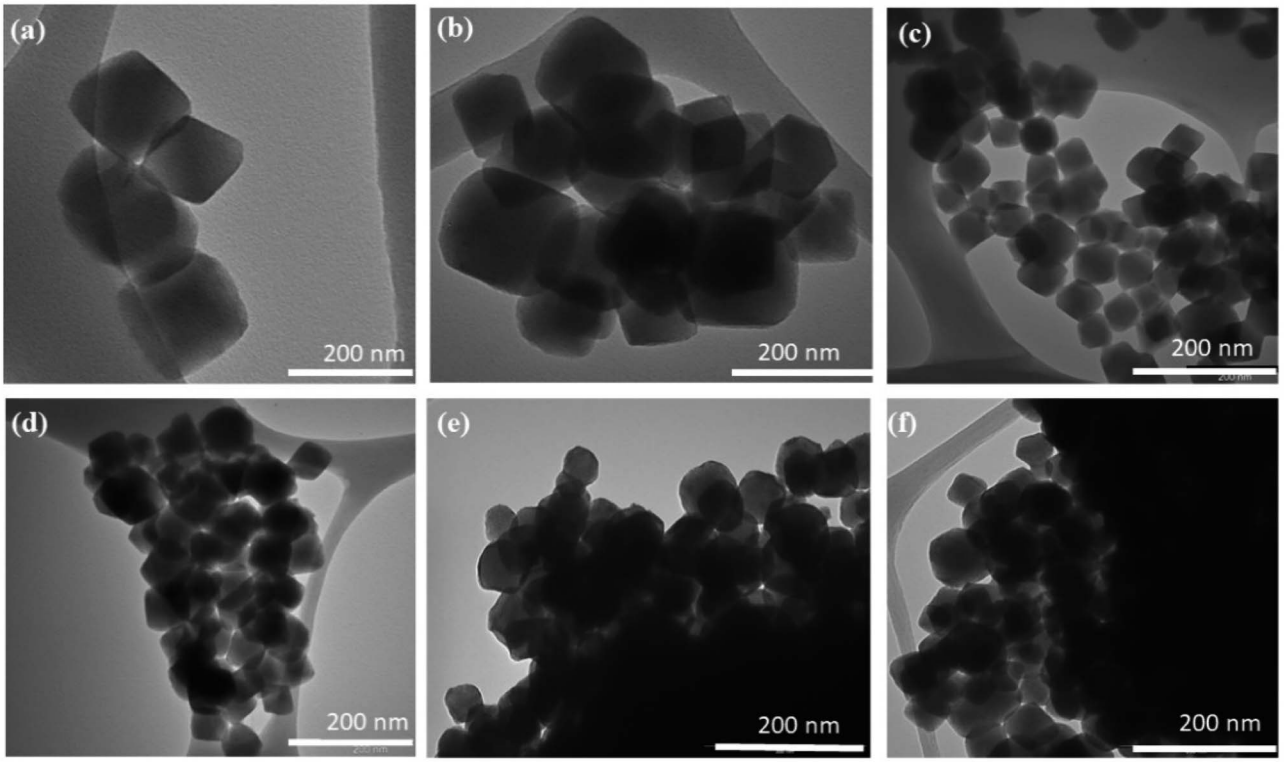

Fig. 2 The TEM images of the samples (a) pure-UiO-66, (b) 10 mL UiO-66@MoS_2QDs, (c) 15 mL UiO-66@MoS_2QDs, (d) 20 mL UiO-66@MoS_2QDs, (e) 25 mL UiO-66@MoS_2QDs, and (f) 30 mL UiO-66@MoS_2QDs.

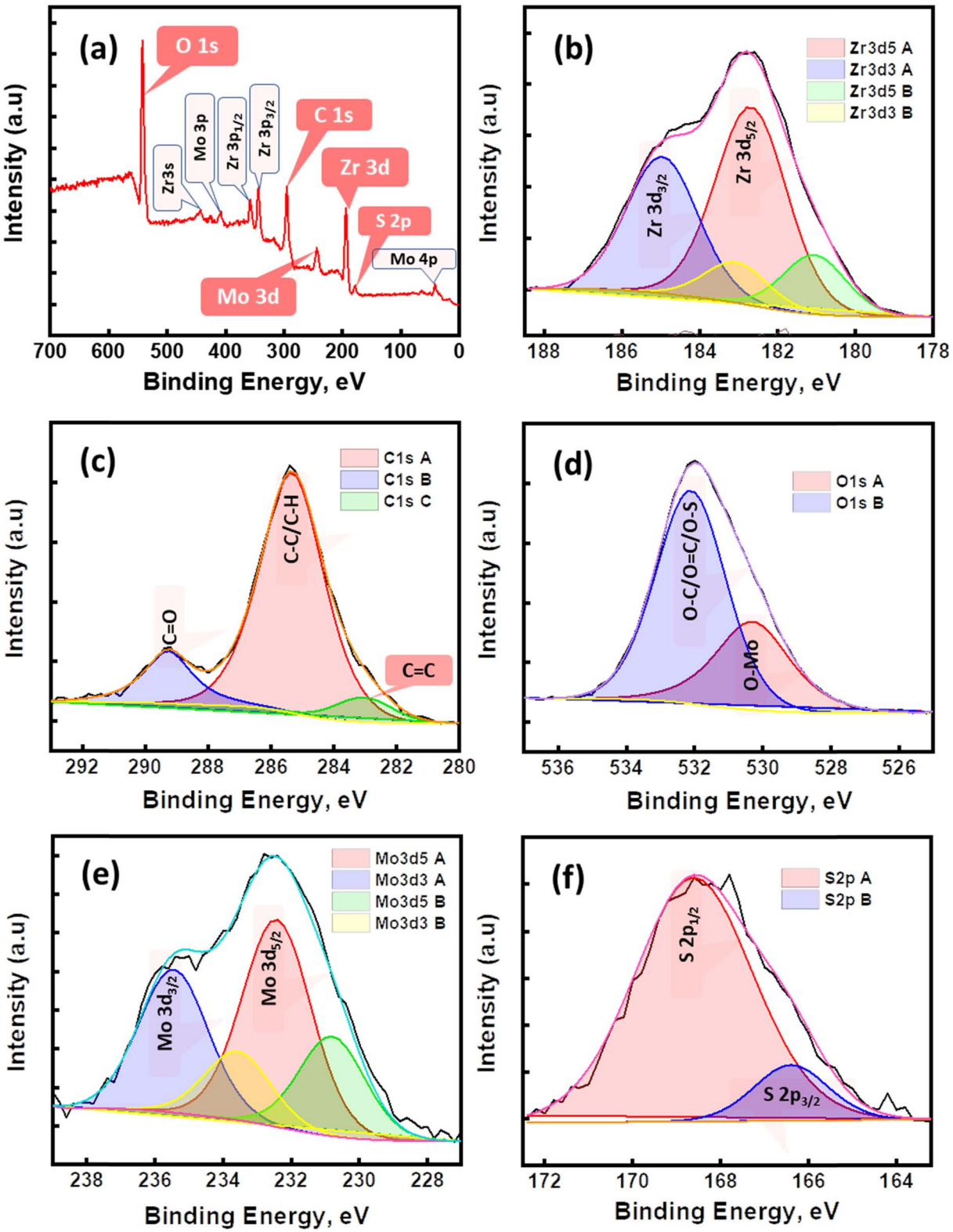

Fig. 3 The XPS spectra of 15 mL UiO-66@MoS_2QDs: (a) survey spectra, (b) Zr 3d, (c) C 1s, (d) O 1s, (e) Mo 3d, and (f) S 2p.

XPS analysis was carried out to explore the surface valence state plus the elemental structure of the 15 mL UiO-66@MoS_2-QDs photocatalyst, as shown in Fig. 3. The survey spectrum (Fig. 3a) proved the elemental components of MoS_2QDs@UiO-66, where the peaks of zirconium (Zr 3d), carbon (C 1s), oxygen (O 1s), molybdenum (Mo 3d), and sulfur (S 2p) were obtained, proving the presence of MoS_2QDs along the surface of UiO-66 matrix. The peaks shown in Fig. 3b, at the binding

Table 1 The element analysis of UiO-66 coatings at different concentrations of MoS_2QDs by XRF

Sample	Element	Atomic ratios (at%)
UiO-66	Zr	100
10 mL MoS_2QDs@UiO-66	Zr	74.89
	Mo	6.28
	S	18.83
15 mL MoS_2QDs@UiO-66	Zr	54.76
	Mo	8.64
	S	36.60
20 mL MoS_2QDs@UiO-66	Zr	51.38
	Mo	9.64
	S	38.98
25 mL MoS_2QDs@UiO-66	Zr	47.8
	Mo	10.65
	S	41.55
30 mL MoS_2QDs@UiO-66	Zr	44.3
	Mo	11.62
	S	44.08

energies of 184.98 eV and 182.7 eV, could be attributed to Zr $3d_{3/2}$ and Zr $3d_{5/2}$ of UiO-66 in the UiO-66@MoS_2QDs photocatalyst, respectively. In the C 1s spectrum (Fig. 3c), the C=O, C–C/C–H, and C=C bonds appeared at 289.27 eV, 285.3 eV, and 282.9 eV, respectively. Fig. 3d shows two clear peaks at 530.2 and 532.1 eV in the O 1s spectrum, these peaks could be named the O–Mo bonds and O–C/O=C/O–S bonds as a result of MoS_2QDs grafting with the UiO-66 platform. The Mo 3d spectrum data is shown in Fig. 3e. Two characteristic peaks at 235.4 eV (Mo $3d_{3/2}$) and 232.4 eV (Mo $3d_{5/2}$) are attributed to the Mo(IV) oxidation states of MoS_2. On the other hand, there are two additional weak peaks at 233.5 eV (Mo $3d_{3/2}$), and 230.8 eV (Mo $3d_{5/2}$) attached to the Mo(VI) oxidation state. The peaks of S $2p_{1/2}$ and S $2p_{3/2}$ binding energies were presented at 168.6 eV and 166.3 eV, respectively, relating to the characteristic values for S^{2-}, as shown in Fig. 3f. These obtained results demonstrated that UiO-66@MoS_2QDs photocatalysts were successfully fabricated.

3.2. Effect of impregnated MoS_2QDs amounts

The photocatalytic activity of UiO-66@MoS_2QDs was assessed by varying the quantity of additional MoS_2QDs added. The UV-vis absorption spectra of MB (at λ_{max} 665 nm) before and after stirring with UiO-66 and UiO-66@MoS_2QDs are explained in Fig. 4a–f. With the increasing exposure time, the intensity of the MB peak was decreased. The photocatalytic performance of UiO-66@MoS_2QDs composites is superior to that of pure UiO-66. Fig. 4a shows that the effectiveness of MB degradation by UiO-66's was approximately 49.5%. In the case of the UiO-66@MoS_2QDs photocatalyst, the photocatalytic performance improved with an increase in the MoS_2QDs contents, where the MB-degradation efficiency was increased to approximately 99% in the case of UiO-66@MoS_2QDs (15 mL) (Fig. 4b and c). Fig. 4d and f show that the photocatalytic performance of the photocatalyst towards MB dye decreased upon increasing the number of MoS_2QDs. Initially, the photocatalytic degradation of MB was improved by the addition of a modest quantity of MoS_2QDs; however, this effect was quickly reversed by an increase in the MoS_2QDs content. However, the UiO-66@MoS_2QDs experiment had too many MoS_2QDs. The higher amount of photo-generated electrons is responsible for this. The photocatalytic performance was, however, reduced as the number of MoS_2QDs increased. Because of the extra MoS_2QDs, the composites are inclined to aggregation.[26] As a result, the high concentrations of MoS_2QDs in a composite may probably increase the likelihood of recombination of photo-generated electron–hole pairs in the composite.[27] As a result of this test, 15 mL UiO-66@MoS_2QDs was selected for the next experiments.

3.3. Optimizing of the MB-photocatalytic decomposition

The precise mechanism by which photocatalyst degrades the MB dye is unknown because it is dependent on various experimental setup parameters, such as the pH of the solution, photocatalyst dosage, solution temperature, period of irradiation, the concentration of MB-pollutant, and presence of co-existing ions. The primary objective of this work is to validate how the factors listed above affect the efficacy of MB degradation under UV irradiation.

The pH of the photocatalytic medium influences the % photocatalytic degradation efficiency owing to it altering the surface charge of UiO-66@MoS_2QDs during ionization of the surface functional groups. The percent degradation efficiency of photocatalysis is represented as a percentage. The anionic dye molecule is transformed into anionic chloride ions, in this example, which are subsequently converted back to the anionic dye molecules. As a consequence, MB exists as a positively charged ion when the pH is higher than seven.[28] When 25 mg of UiO-66@MoS_2QDs was mixed in fifty ml of MB-solution (ten ppm) for 30 minutes at RT, it was discovered that the solution's pH used influenced the photocatalytic degradation of MB. It was necessary to employ buffer solutions to adjust the pH of the MB solutions from 2 to 10. When the pH of the photocatalytic medium was increased, it was found that the MB quantity was reduced by the photocatalytic medium (as shown in Fig. 5a). The outer surface of MoS_2QDs@UiO-66 was transformed into a charged surface when the pH was raised to 7. It is hypothesized that these protonated active sites would inhibit the interaction of cationic MB molecules with UiO-66@MoS_2QDs, hence slowing down MB degradation. When pH levels are acidic, it has been shown that the breakdown rate of the cationic MB molecules is lowered as a result of competition between H^+ ions and MB molecules for available active sites.[29] As the pH is reduced below 7, the surface of the UiO-66@MoS_2QDs becomes negative, increasing the adsorption of cationic MB-molecules, and hence the proportion of the MB-dye is destroyed. This resulted in a favorable breakdown of MB using UiO-66@MoS_2QDs in an alkaline pH medium. Because the difference between pH 7 and pH 7 is very small, it was established that pH 7.0 gave the best MB degradation; hence, more photocatalytic tests were conducted at this pH value.

The quantity of the applied photocatalyst affects the photocatalytic activity and MB degradation. This was performed by increasing the amount of UiO-66@MoS_2QDs from 10 to 50 mg,

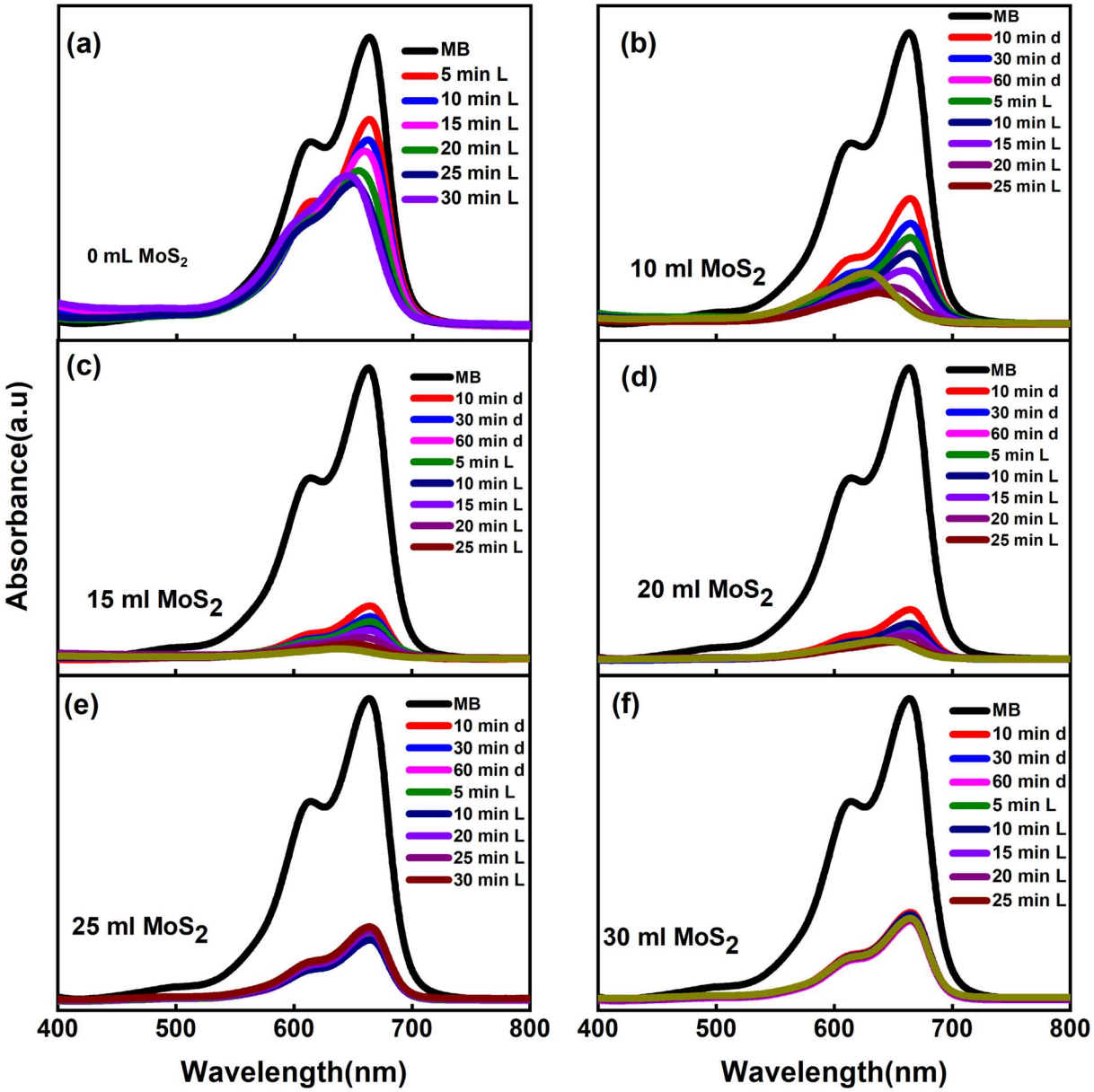

Fig. 4 (a) The UV-vis absorption spectrum of UiO-66, and (b–f) UV-vis absorption spectra of UiO-66@MoS_2QDs at different concentrations of MoS_2QDs (10, 15, 20, 25, and 30 mL).

as shown in Fig. 5b, while maintaining the same MB concentration (10 ppm). The MB-dye solution was spun and irradiated at different concentrations of the photocatalyst for 30 minutes under UV light at pH 7. By increasing the dose of UiO-66@MoS_2QDs, the % photodegradation was increased. Due to the reduced amount of the utilized photocatalyst, the photodegradation percentage was lower due to the deficiency of the surface-active sites in the photocatalyst. Increases in the dosage of UiO-66@MoS_2QDs result in a rise in the UV-exposed area, which results in an increase in the number of photons absorbed by UiO-66@MoS_2QDs and the quantity of the adsorbed MB-molecules in the system. 25 mg of UiO-66@MoS_2QDs displayed good photocatalytic activity under this condition. In future, the UiO-66@MoS_2QDs weight will be eliminated, resulting in a slight increase in catalytic activity. As a consequence, the MB-photodegradation experiment required only 25 mg of UiO-66@MoS_2QDs.

Increased decolorization and removal efficiency may be achieved with increasing temperature. As demonstrated in Fig. 5c, the temperature had a significant impact on MB degradation's performance. By increasing the system temperature (from 298 to 333 K), the degradation percentage of MB increased from 97% to 99.5%. A possible explanation for this trend is an increase in the dispersion and crashing of the key radicals and ions due to the increase in the temperature of the system, which increases the percentage of MB degradation. Another factor that influences the creation of OH is temperature, which may either speed up or slow it down.[30] Since there is

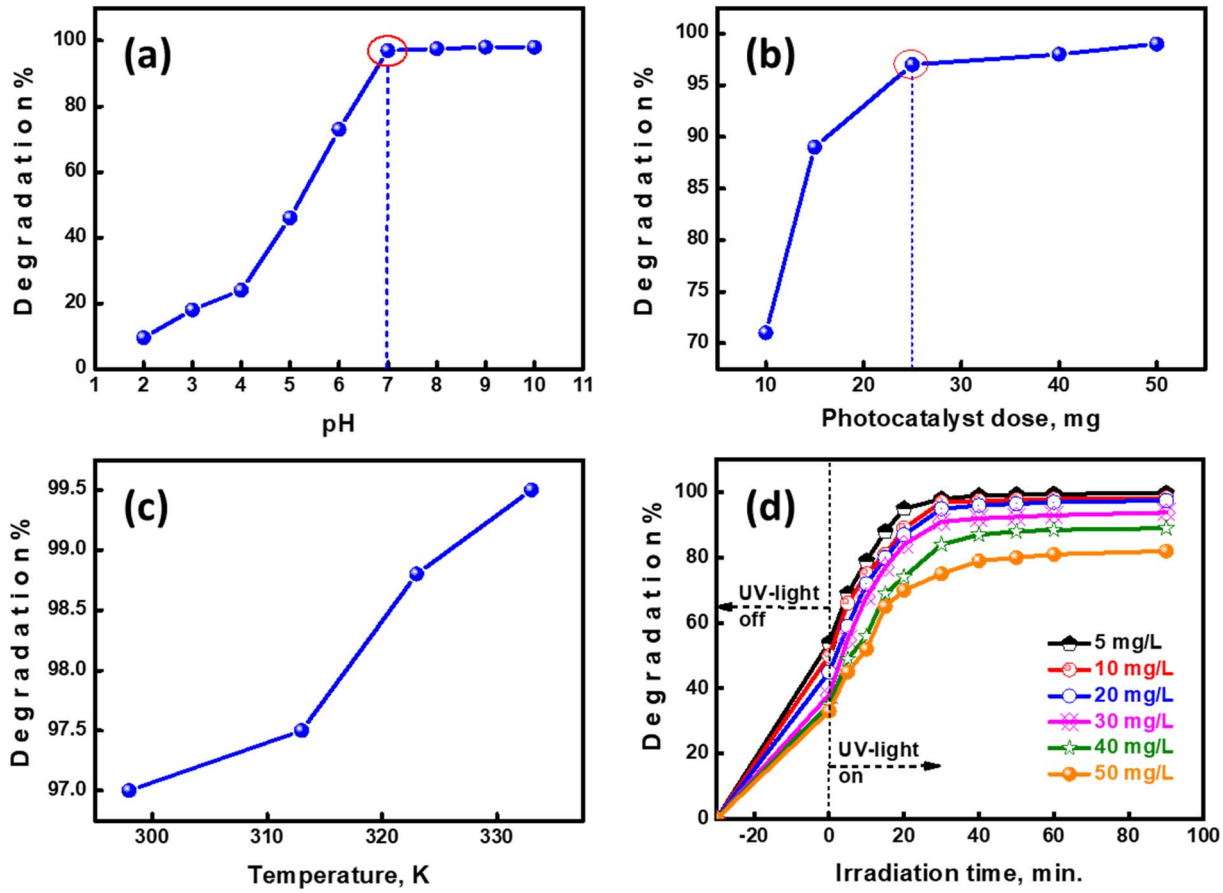

Fig. 5 The effect of (a) pH, (b) photocatalyst dose, (c) temperature, and (d) CV-concentration on the MB-photocatalytic degradation using UiO-66@MoS_2QDs.

only a 2.5% difference in the MB degrading efficiency between 298 K and a high temperature, the high temperature might not be profitable because of the additional heat energy costs.

While leaving other parameters constant, such as 25 mg UiO-66@MoS_2QDs dosage, 50 mL MB-solution, pH 7, and room temperature, we examined the effect of a lower initial MB concentration (5 to 50 ppm). As exhibited in Fig. 5d, the preliminary MB concentration increased as the MB decolourization percentage reduced. Because the path length of photons through the MB's solution was reduced and the active surface sites of UiO-66@MoS_2QDs were protected, this behaviour is adequate. This process results in a reduction in the ultraviolet radiation amount absorbed using MoS_2QDs@UiO-66 particles, which in turn decreases the electron–hole pair formation (*i.e.*, reactive radicals), lowering the amount MB photodegradation%.[31] This means that the solution of the MB dye with a UiO-66@MoS_2QDs photocatalyst should have a concentration of 10 ppm or less. Fig. S1† shows that the MB-adsorption capacity of UiO-66@MoS_2QDs was enhanced with an extended initial concentration of MB until it reached the maximum adsorption capacity. The adsorbed amount of MB was found to be 46.5 mg g^{-1} using the following equation q_e (mg g^{-1}) = $(C_i - C_f)(V/m)$. Where C_i and C_f (ppm) are the initial and final MB concentrations; V is the volume of the MB solution (L), and w (g) is the mass of UiO-66@MoS_2QDs.

3.4. Mechanism of MB-photocatalytic degradation

To examine the effect of MoS_2QDs on the optical properties of the MoS_2QDs@UiO-66 photocatalyst, UV-vis spectra of the pure UiO-66 and UiO-66 coatings with different ratios of MoS_2QDs heterostructure were investigated. Nevertheless, the UiO-66@MoS_2QDs spectrum showed a change in the absorption at the UV-vis region, indicating that the quantum dot MoS_2 effect on the absorption spectrum, mainly in the visible region of 400–600 nm. The energy gap (E_g) of all the active materials was computed utilizing Tauc's relation.[32] MoS_2QDs influence the energy gap of the UiO-66 and range from 3.66 to 4.05 eV, as shown in Fig. 6b. The absorption enhancement of the UiO-66@MoS_2QDs nanocomposites in the visible region may improve the photoelectron–hole pairs generation that takes part in the reaction, which is appropriate for the photocatalytic route.

As a consequence of the exposure of the UiO-66@MoS_2QDs photocatalyst to ultraviolet light with $h\nu$ higher than the E_g of UiO-66@MoS_2QDs, electrons (e^-) in the VB can be transferred to a higher energy level (CB), resulting in the formation of positive holes (h^+) at the VB level. Electron–hole recombination is reduced, which is a crucial component in improving the photocatalytic efficiency of the system. The e^- and h^+ ions can be used to begin reactions between activated-e^- and oxygen, which can result in the creation of a free radical such as $O_2^{\bullet -}$ in the presence of oxygen. This reaction resulted in the formation

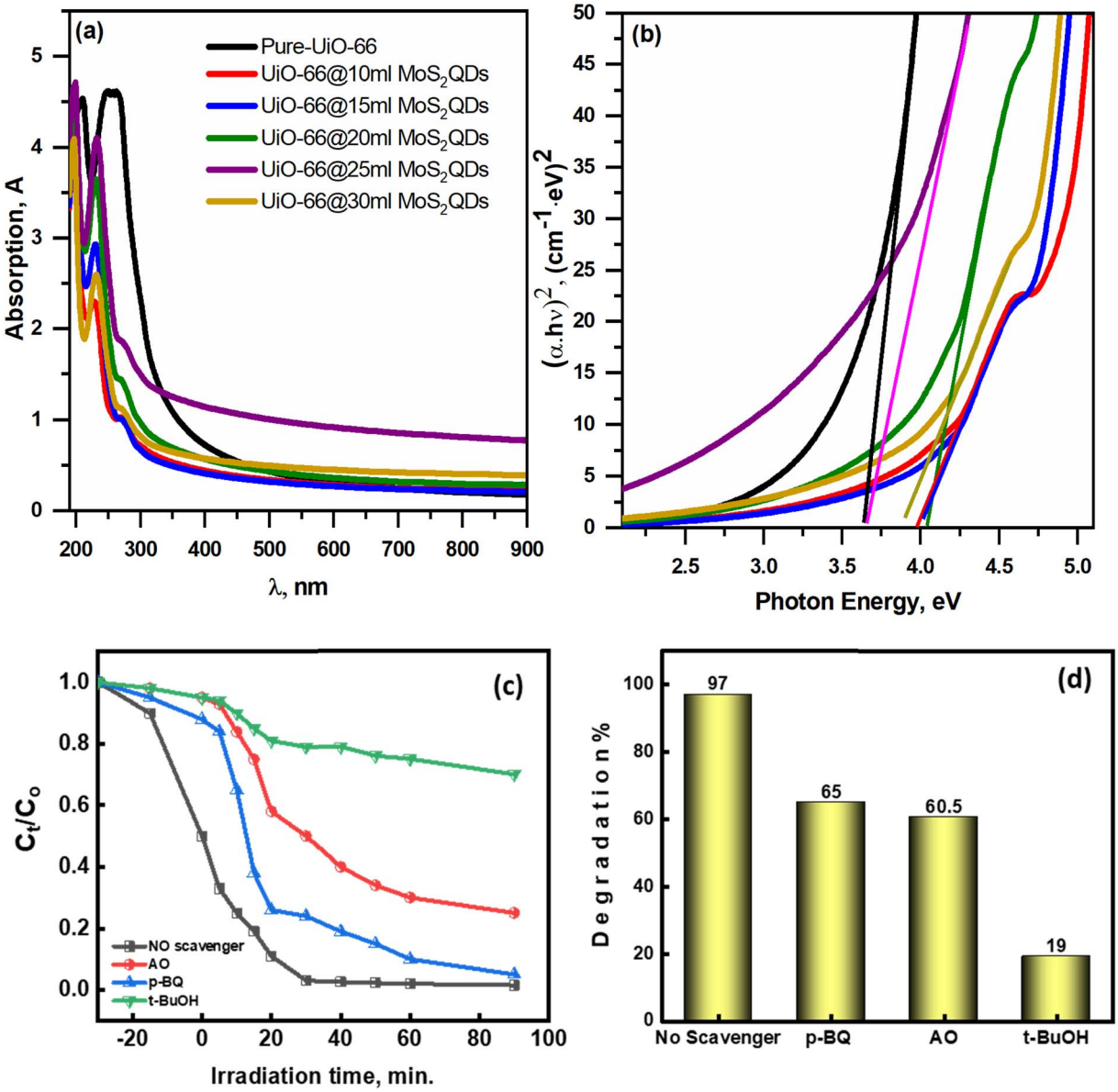

Fig. 6 (a) The UV-vis spectra and (b) Tauc plots of pure UiO-66 NPs and UiO-66@MoS_2QDs nanocomposites. The impact of various scavengers on the photocatalytic degradation of MB dye (c and d).

of free radicals ($OH^{\bullet}$), which are beneficial for the photocatalytic degradation of MB because they have a high oxidative capacity, which allows for the breakdown of larger molecules into smaller molecules and less damaging and harmless species, such as CO_2 and H_2O, are formed.[33] Superoxide can enhance photodegradation by preventing pair recombination of e^-–h^+ couples. To investigate the active species responsible for MB-photocatalytic degradation using UiO-66@MoS_2QDs, many tests were performed using several scavengers, such as *p*-benzoquinone (*p*-BQ), *tert*-butyl alcohol (*t*-BuOH), and ammonium oxalate (AO) to trap $O_2^{\bullet-}$ $OH^{\bullet}$ radicals, and h^+, respectively. *p*-BQ, AO, and *t*-BuOH were added to the MB solution under optimal degradation conditions. Fig. 6c and d suggested that adding AO and *p*-BQ has little effect on the MB degradation performance, referring to h^+ and $O_2^{\bullet-}$ radicals having no significant impact on MB degradation. On the other hand, adding *t*-BuOH clearly decreases the MB-degradation rate. Therefore, $OH^{\bullet}$ radicals are the main active species in the photocatalytic degradation of MB dye. The photodegradation of UiO-66@MoS_2QDs may be characterized using the following equations:

$$\text{UiO-66@MoS}_2\text{QDs-66} + h\nu \rightarrow \text{UiO-66@MoS}_2\text{QDs} + e^- + h^+$$

$$e^- + O_2 \rightarrow O_2^{\bullet-}$$

$$H_2O + h^+ \rightarrow HO^{\bullet} + H^+$$

$$O_2^{\bullet-} + HO^{\bullet} + H^+ + \text{MB} \rightarrow \text{micromolecules} + CO_2 + H_2O$$

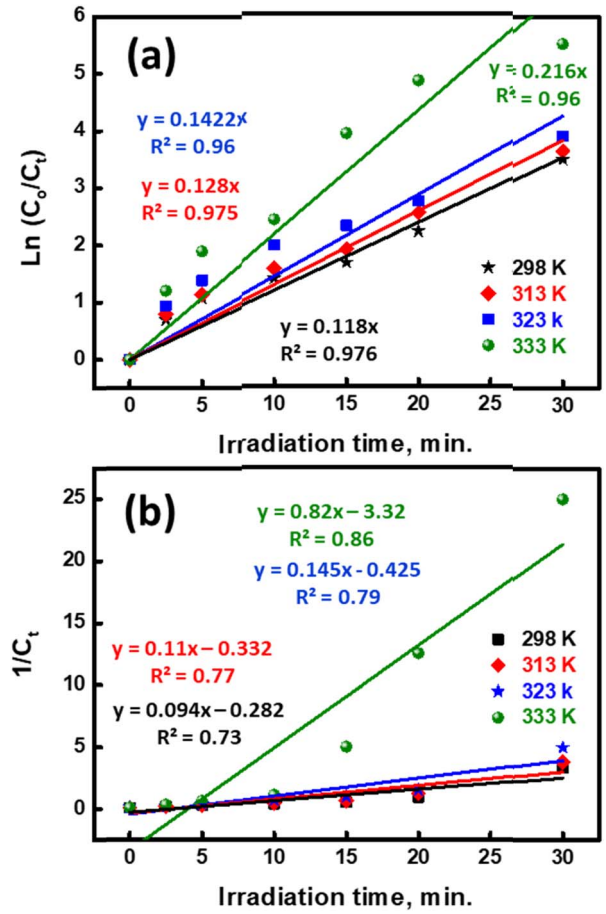

Fig. 7 The kinetic study of MB-photodegradation using UiO-66@MoS_2QDs through pseudo 1st order (a) and pseudo 2nd order (b) kinetic models.

Table 2 The parameters of pseudo 1st order (A) and pseudo 2nd order (B) kinetic models for MB-photodegradation using the UiO-66@MoS_2QDs photocatalyst

	Temperature K	R^2	Rate constant (K)	$T_{0.5}$, min
Pseudo 1st order	298	0.976	0.118	5.87
	313	0.975	0.128	5.41
	323	0.96	0.1422	4.87
	333	0.96	0.216	3.2
Pseudo 2nd order	298	0.73	0.094	1.06
	313	0.77	0.11	0.91
	323	0.79	0.145	0.69
	333	0.86	0.82	0.122

3.5. Kinetic study of the photocatalytic degradation of MB dye

To explore the kinetic of MB-photocatalytic degradation process by UiO-66@MoS_2QDs, pseudo 1st and 2nd order kinetics styles were studied at the optimum degradation conditions (dose 25 mg, volume 50 mL, concentration 10 ppm, and pH 7), where temperature and irradiation time were variables. The pseudo 1st and 2nd order kinetics models can be demonstrated in the following reactions:[23,33]

$$\mathrm{Ln}\left(\frac{C_o}{C_t}\right) = K_1 t$$

$$\frac{1}{C_t} - \frac{1}{C_o} = K_2 t$$

The pseudo-first- and second-order rate constants are indicated by the letters K_1 (min^{-1}) and K_2 (g mg^{-1} min^{-1}), respectively. °C represents the initial MB concentration, whereas C_t represents the cumulative MB concentration (t, min). To establish the % photodegradation of MB dye at various temperatures, researchers examined photodegradation kinetic models, such as those shown in Fig. 7a and b. The correlation coefficients (R^2), rate constants (K_1 and K_2), and half-life time associated with the fitted prototypes are listed in Table 2. The half-life time ($t_{0.5}$, min) for pseudo-1st and 2nd orders may be determined using the ($0.693/K_1$) and ($1/K_2C_o$) formulas, respectively. The R^2 value of the pseudo-first-order degradation kinetic prototype ($\ln(C_o/C_t)$ *vs.* t) was much larger than that of the pseudo-second-order model ($1/C_t$ *vs.* t), indicating that the pseudo-first-order model was more accurate. As a consequence, the pseudo-first-order model can properly represent the MB-

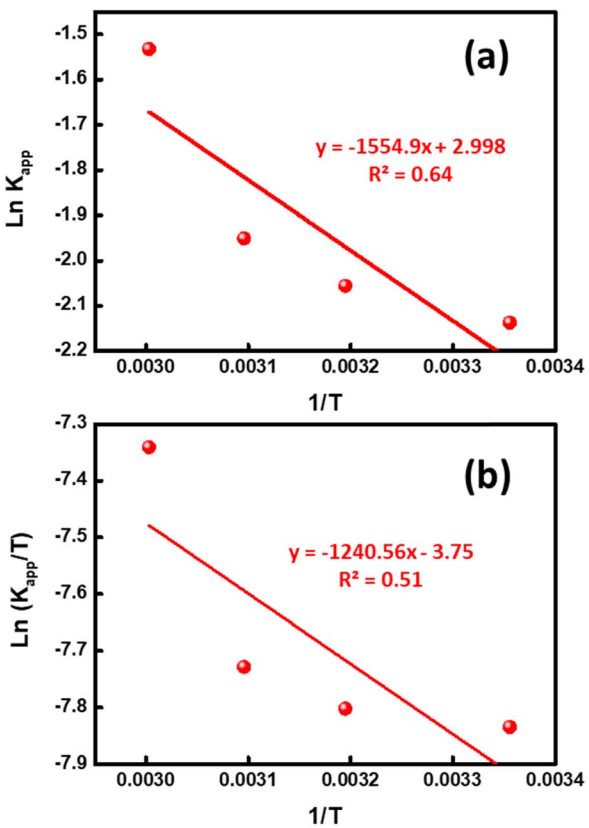

Fig. 8 (a) The plots of ln K_{app} *vs.* $1/T$ and (b) $\ln(K_{app}/T)$ *vs.* $1/T$ for the MB degradation using the UiO-66@MoS_2QDs photocatalyst.

Table 3 The thermodynamic parameters for MB degradation using the UiO-66@MoS_2QDs photocatalyst

Temperature K	The rate constant (K)	R^2	E_a, kJ mol^{-1}	ΔH, kJ mol^{-1}	ΔS, J mol^{-1} K^{-1}	ΔG, kJ mol^{-1}
298	0.118	0.976	12.927	10.314	−228.47	78.398
313	0.128	0.975				81.825
323	0.1422	0.96				84.109
333	0.216	0.96				86.394

photodegradation of UiO-66@MoS_2QDs in this study. The MB-degradation rate constant of UiO-66@MoS_2QDs at 333 K is higher than that of UiO-66@MoS_2QDs at 323 K > 313 K > 298 K, showing better photocatalytic activity of MB dye under UV-irradiation at high temperature.

3.6. Thermodynamic study of MB photocatalytic degradation

To compute the activation energy (E_a) and other parameters of the thermodynamics, we utilized the fluctuation of K_1 with temperature (303, 313, 323, and 333 K). The Arrhenius equation was utilized to compute the degradation's activation energy:[34]

$$\ln K_{app} = -\frac{E_a}{RT} + \ln A$$

Here, K_{app} is the constant of the apparent rate (min^{-1}), R is Arrhenius (min^{-1}), A is the universal gas constant (J mol^{-1} K^{-1}), and T is the temperature (K). A straight line was drawn between ln(K_{app}) and 1/T, and from its slope, we were able to compute the activation energy, as illustrated in Fig. 8a. The activation energy was 12.927 kJ mol^{-1}, which is a moderate amount. This indicated that the oxidative process had a low barrier to entry. The photocatalytic decomposition of MB is physical in nature since activation energies of less than 20 kJ mol^{-1} were found in the experiment findings.[35] The following equations were used to calculate the thermodynamic characteristics based on the results from the degradation tests at 298, 313, 323, and 333 K:[34]

$$\ln \frac{K_{app}}{T} = \frac{-\Delta H^{\circ}}{RT} + \ln \frac{K_B}{\hbar} + \frac{\Delta S^{\circ}}{R}$$

$$\Delta G^{\circ} = \Delta H^{\circ} - T\Delta S^{\circ}$$

where K_B is a Boltzmann constant 1.3806 × 10^{-23} m^2 kg s^{-2} K^{-1}. $\Delta H°$, $\Delta S°$, and $\Delta G°$ are enthalpy (J mol^{-1}), entropy (J mol^{-1} K^{-1}) and Gibbs free energy (J mol^{-1}), respectively, while $\hbar$ is the Planck constant 6.626 × 10^{-34} m^2 kg s^{-1}. To calculate $\Delta H°$, $\Delta S°$, and $\Delta G°$ values, ln(K_{app}/T) was plotted *versus* (1/T), as shown in Fig. 8b. The obtained data of the thermodynamic parameters are given in Table 3. The reduction in unpredictability in the system where deterioration occurred is shown by the negative $\Delta S°$ value (−228.47 J mol^{-1} K^{-1}). As an alternative, due to the positive enthalpy values (10.31 kJ mol^{-1}), the MB degrading process utilizing UiO-66@MoS_2QDs photocatalyst is endothermic. The negative value of $\Delta G°$ specifies that the photocatalytic degradation process is a non-spontaneous process, where the MB-degradation process requires an input of energy to take place.

3.7. Recycling and reusability of the spent UiO-66@MoS_2QDs photocatalyst

Photocatalytic degradation may be employed to renew and reuse the wasted UiO-66@MoS_2QDs photocatalyst, hence reducing the total cost of the MB removal process. Thus, the recovery of the spent UiO-66@MoS_2QDs photocatalyst was evaluated using centrifugation, decanting, and washing with deionized water. The ultrasonic and 0.1 M HNO_3 washing conditions ensured that the MB dye was eliminated and decaying components were removed during the photocatalytic process. Drying at 80 °C was used to remove water from the final

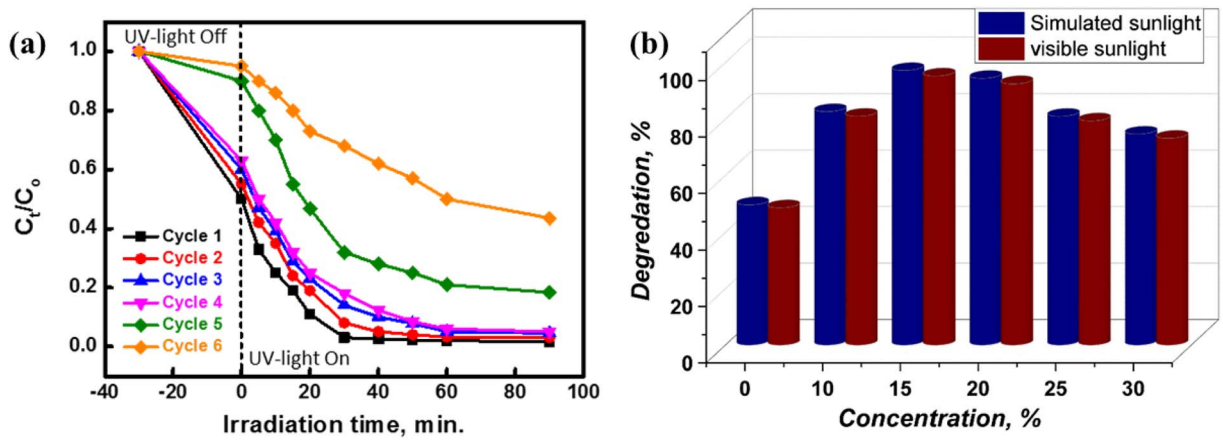

Fig. 9 (a) Recycling of the spent UiO-66@MoS_2QDs for six reuse cycles and (b) comparison between the degradation efficiency of the catalytic activity at different concentrations of MoS_2 QDs coated with UiO-66 under real sunlight and simulated sunlight.

product. The regenerated UiO-66@MoS_2QDs can be utilized again for a fresh cycle of regeneration. The photostability of the UiO-66@MoS_2QDs was tested over six cycles. Using the heterosystem shown in Fig. 9a, the activity of the UiO-66@MoS_2QDs structure decreased by less than 10% after the fourth cycle, illustrating the extremely reusable nature of the material. There may be a concentration of the pollutant molecules on the active sites on the surface of the UiO-66@MoS_2QDs that is reducing photodegradation. To be more realistic, we applied the photocatalytic performance of the UiO-66 coated with different concentrations of MoS_2QDs in real sunlight. Since the experiment of the photocatalyst of MB dye was performed under outside solar light on a sunny day in October from 12 a.m. and 3 p.m., where the solar intensity is 7.2–7.8 kW h per m^2 per day in Al-Azhar University, Assiut, Egypt, there was no significant difference between both simulated and real sunlight. The best concentration was 15 mL MoS_2 QDs for removal on that day, and it was around 99% for simulated sunlight and 97% for real sunlight, as demonstrated in Fig. 9b.

4. Conclusion

A facile and low-cost route was used to construct a heterostructure of UiO-66 coated by MoS_2QDs *via* the ultrasonication method. X-ray diffraction proved that all samples had a single cubic phase of UiO-66 without any additional contaminations from other phases. Morphological measurements (TEM) exhibited the formation of UiO-66@MoS_2QDs and the distribution of MoS_2QDs on the surface of UiO-66. The photocatalysis performance of UiO-66 was enhanced by increasing the concentration of MoS_2QDs up to 15 mL and then decreased by increasing the quantity of MoS_2QDs, indicating that the best concentration was 15 mL, which could remove more than 99% of the MB dye within 30 min. The photocatalytic performance of the 15 mL concentration was 97% for real sunlight. The outcomes showed that the proposed photocatalyst retained its performance to remove MB pollutants even after numerous reuse cycles. The current work offers a low-cost, advanced heterostructure, and straightforward photocatalyst manufacturing technique for water purification.

Author contributions

Abdelaziz M. Aboraia: writing – original draft, preparation, and editing. Majd Al-omoush: writing – original draft, preparation and editing. Malak Solayman: validation, software, writing – review & editing. Hatem M. H. Saad: methodology, data curation, writing – original draft, characterization part. Gomaa Khabiri, preparation and editing. M. Saad & Ghalyah M. Alsulaim, methodology, data curation, writing – original draft. Alexander V. Soldatov, review & editing. Yasser A. M. Ismail and H. Gomaa: calculation, review, and writing the manuscript.

Conflicts of interest

The authors have no competing interests to declare that are relevant to the content of this article.

Acknowledgements

The authors extend their appreciation to the Deanship of Scientific Research at King Khalid University for funding this work through a large group Research Project under grant number RGP2/289/44. The authors extend their appreciation to King Khalid University for their continuous support throughout the research.

References

1 Y. Shi, J. Ma, Y. Chen, Y. Qian, B. Xu, W. Chu and D. An, *Sci. Total Environ.*, 2022, **804**, 150024.
2 Y. Miao, L. Liu, Y. Zhang, Q. Tan and J. Li, *J. Hazard. Mater.*, 2022, **425**, 127900.
3 S. Tiwari, S. Kumar and A. K. Ganguli, *J. Photochem. Photobiol., A*, 2022, **424**, 113622.
4 H. He, Z. Luo and C. Yu, *J. Alloys Compd.*, 2020, **816**, 152652.
5 H. He, Z. Luo, Z.-Y. Tang and C. Yu, *Appl. Surf. Sci.*, 2019, **490**, 460–468.
6 J. Xue, M. Xu, J. Gao, Y. Zong, M. Wang and S. Ma, *Colloids Surf., A*, 2021, **628**, 127288.
7 T. Xia, Y. Lin, W. Li and M. Ju, *Chin. Chem. Lett.*, 2021, **32**, 2975–2984.
8 C. Du, Z. Zhang, G. Yu, H. Wu, H. Chen, L. Zhou, Y. Zhang, Y. Su, S. Tan, L. Yang, J. Song and S. Wang, *Chemosphere*, 2021, **272**, 129501.
9 H. He, L. Zeng, X. Peng, Z. Liu, D. Wang, B. Yang, Z. Li, L. Lei, S. Wang and Y. Hou, *Chem. Eng. J.*, 2023, **451**, 138628.
10 A. Al Obeidli, H. B. Salah, M. Al Murisi and R. Sabouni, *Int. J. Hydrogen Energy*, 2022, **47**, 2561–2593.
11 J. He, J. Wang, Y. Chen, J. Zhang, D. Duan, Y. Wang and Z. Yan, *Chem. Commun.*, 2014, **50**, 7063–7066.
12 A. Zada, M. Khan, M. A. Khan, Q. Khan, A. Habibi-Yangjeh, A. Dang and M. Maqbool, *Environ. Res.*, 2021, **195**, 110742.
13 A. Kidanemariam, J. Lee and J. Park, *Polymers*, 2019, **11**(12), 2090.
14 T. K. Vo, J. Kim, T. H. Vu, V. C. Nguyen and D. T. Quang, *Sep. Purif. Technol.*, 2022, **283**, 120237.
15 Z. Man, Y. Meng, X. Lin, X. Dai, L. Wang and D. Liu, *Chem. Eng. J.*, 2022, **431**, 133952.
16 G. Jajko, J. J. Gutiérrez-Sevillano, A. Sławek, M. Szufla, P. Kozyra, D. Matoga, W. Makowski and S. Calero, *Microporous Mesoporous Mater.*, 2022, **330**, 111555.
17 V. V. Butova, A. M. Aboraia, M. Solayman, I. S. Yahia, H. Y. Zahran, A. F. Abd El-Rehim, H. Algarni, G. Khabiri and A. V. Soldatov, *Microporous Mesoporous Mater.*, 2021, **325**, 111314.
18 L. Ni, Y. Zhu, J. Ma and Y. Wang, *Water Res.*, 2021, **188**, 116554.
19 X. Hao, Z. Jin, H. Yang, G. Lu and Y. Bi, *Appl. Catal., B*, 2017, **210**, 45–56.
20 Y. Zhang, W. Li, Z. Hu, X. Jing and L. Yu, *Chin. Chem. Lett.*, 2023, 108938.
21 V. V. Butova, A. P. Budnyk, K. M. Charykov, K. S. Vetlitsyna-Novikova, A. L. Bugaev, A. A. Guda, A. Damin, S. M. Chavan,

S. Øien-Ødegaard, K. P. Lillerud, A. V. Soldatov and C. Lamberti, *Inorg. Chem.*, 2019, **58**, 1607–1620.
22 G. Khabiri, A. M. Aboraia, M. Soliman, A. A. Guda, V. V. Butova, I. S. Yahia and A. V. Soldatov, *Ceram. Int.*, 2020, **46**, 19600–19608.
23 A. Dasari and V. Guttena, *Mater. Today Commun.*, 2019, **19**, 157–169.
24 M. Liu, Y. Li, L. Yu, Q. Xu and X. Jiang, *Sci. China: Chem.*, 2018, **61**, 294–299.
25 S. E. A. Elashery, I. Ibrahim, H. Gomaa, M. M. El-Bouraie, I. A. Moneam, S. S. Fekry and G. G. Mohamed, *Magnetochemistry*, 2023, **9**(2), 56.
26 Y. Ding, Y. Zhou, W. Nie and P. Chen, *Appl. Surf. Sci.*, 2015, **357**, 1606–1612.
27 J. Li, X. Liu, L. Pan, W. Qin, T. Chen and Z. Sun, *RSC Adv.*, 2014, **4**, 9647–9651.
28 M. Khnifira, S. El Hamidi, M. Sadiq, S. Şimşek, S. Kaya, N. Barka and M. Abdennouri, *Appl. Surf. Sci.*, 2022, **572**, 151381.
29 K. O. Kassem, M. A. T. Hussein, M. M. Motawea, H. Gomaa, Z. A. Alrowaili and M. Ezzeldien, *J. Cleaner Prod.*, 2021, **326**, 129416.
30 K. Ghosh, N. Bar, A. B. Biswas and S. K. Das, *Sustainable Chem. Pharm.*, 2021, **19**, 100370.
31 F. H. Mustapha, A. A. Jalil, M. Mohamed, S. Triwahyono, N. S. Hassan, N. F. Khusnun, C. N. C. Hitam, A. F. A. Rahman, L. Firmanshah and A. S. Zolkifli, *J. Cleaner Prod.*, 2017, **168**, 1150–1162.
32 A. M. El Sayed and G. Khabiri, *J. Electron. Mater.*, 2020, **49**, 2381–2392.
33 S. V. P. Vattikuti, I.-L. Ngo and C. Byon, *Solid State Sci.*, 2016, **61**, 121–130.
34 A. H. Jawad, R. A. Rashid, M. A. M. Ishak and L. D. Wilson, *Desalin. Water Treat.*, 2016, **57**, 25194–25206.
35 K. Sharma, R. K. Vyas and A. K. Dalai, *J. Chem. Eng. Data*, 2017, **62**, 3651–3662.